JEM

Article

Ablation of endothelial VEGFR1 improves metabolic dysfunction by inducing adipose tissue browning

Takahiro Seki,[1] Kayoko Hosaka,[1] Carina Fischer,[1] Sharon Lim,[1] Patrik Andersson,[1] Mitsuhiko Abe,[1] Hideki Iwamoto,[1] Yanyan Gao,[2] Xinsheng Wang,[2] Guo-Hua Fong,[3] and Yihai Cao[1,2]

[1]Department of Microbiology, Tumor and Cell Biology, Karolinska Institute, Stockholm, Sweden
[2]Central Research Laboratory, Affiliated Hospital of Qingdao University, Qingdao, China
[3]Center for Vascular Biology, Department of Cell Biology, University of Connecticut Health Center, Farmington, CT

Angiogenesis plays an instrumental role in the modulation of adipose tissue mass and metabolism. Targeting adipose vasculature provides an outstanding opportunity for treatment of obesity and metabolic disorders. Here, we report the physiological functions of VEGFR1 in the modulation of adipose angiogenesis, obesity, and global metabolism. Pharmacological inhibition and genetic deletion of endothelial VEGFR1 augmented adipose angiogenesis and browning of subcutaneous white adipose tissue, leading to elevated thermogenesis. In a diet-induced obesity model, endothelial-VEGFR1 deficiency demonstrated a potent anti-obesity effect by improving global metabolism. Along with metabolic changes, fatty liver and insulin sensitivity were also markedly improved in VEGFR1-deficient high fat diet (HFD)–fed mice. Together, our data indicate that targeting of VEGFR1 provides an exciting new opportunity for treatment of obesity and metabolic diseases, such as liver steatosis and type 2 diabetes.

INTRODUCTION

Obesity and its related metabolic disorders are major health issues affecting all age groups (Spiegelman and Flier, 2001; Zimmet et al., 2001; Després and Lemieux, 2006). Unlike most other tissues in the body, adipose tissue, especially white adipose tissue (WAT), relentlessly undergoes expansion and shrinkage in response to metabolic demands. Under physiological conditions, brown adipose tissue (BAT) possesses an exceptionally high number of microvessels, rendering this tissue one of the most highly vascularized tissues in the body (Cao, 2007, 2010; Yang et al., 2013). The adipose vascular density can be further increased upon metabolic activation, such as cold- or drug-induced browning and nonshivering thermogenesis (Xue et al., 2009; Dong et al., 2013; Seki et al., 2016). Blood vessels are thought to play an adoptive role in coping with metabolic changes of adipocytes (Asano et al., 1997; Tonello et al., 1999). However, this view has recently been changed by the fact that adipose vasculature also play a prominent role in controlling adipocyte functions (Yang et al., 2013; Seki et al., 2016). For example, under cold exposure, endothelial cells (ECs) in angiogenic vessels produce paracrine factors to control browning of subcutaneous WAT (subWAT) and visceral WAT (visWAT; Yang et al., 2013; Seki et al., 2016). In addition to paracrine regulation, cells of the vessel wall, including endothelial and perivascular cells, also serve as a reservoir of stem cells for differentiation into preadipocytes and, subsequently, adipocytes (Tang et al., 2008; Tran et al., 2012).

To switch on an angiogenic phenotype, adipocytes, and likely other cell types in the adipose microenvironment, produce high levels of angiogenic factors. Vascular endothelial growth factor (VEGF) is expressed in adipose tissues and its expression is elevated under a browning condition (Sung et al., 2013; During et al., 2015). It has been reported that VEGF induces a browning phenotype in the adipose tissue (Xue et al., 2009; Sun et al., 2012; Sung et al., 2013; Seki et al., 2016). VEGF binds to its tyrosine kinase receptors, VEGFR1 and VEGFR2, to display various biological functions (Ferrara et al., 2003; Cao, 2009; Shibuya, 2014). Although expression of VEGFR2 is relatively restricted to vascular ECs, VEGFR1 is widely expressed in non-ECs (Shibuya, 2006). It is generally believed that VEGFR2 is the functional receptor that transduces signals for angiogenesis, vascular permeability, vascular survival, and remodeling (Cao, 2009). In contrast to VEGFR2, biological functions of VEGFR1 remain largely undefined although numerous studies claim controversial findings (Lyden et al., 2001; Autiero et al., 2003; Boulton et al., 2008; Li et al., 2015; Otowa et al., 2016). Within the VEGF family, VEGF (also called VEGF-A), placental growth factor (PlGF), and VEGF-B are all able to bind to VEGFR1 (Cao, 2009). Very recently, VEGF-B was reported to induce angiogenesis through the VEGFR1 signaling pathway in adipose tissue (Robciuc et al., 2016). However, the molecular mechanisms that underlie the VEGFR1-mediated signaling are still unclear. It is

Correspondence to Yihai Cao: yihai.cao@ki.se

The Rockefeller University Press
J. Exp. Med. 2018 Vol. 215 No. 2 611–626
https://doi.org/10.1084/jem.20171012

also unclear whether VEGF-B acts directly on adipocytes through VEGFR1 to induce metabolic changes.

In this study, we took powerful genetic approaches to specifically delete VEGFR1 from vascular ECs without impairing this receptor signaling in other cell types. Furthermore, we employed physiologically relevant animal models without introducing any additional factors or other invasive procedures. Blocking VEGFR1 alone, but not VEGFR2, produced a remarkable browning phenotype of subWAT and visWAT. It was surprising that deletion of EC VEGFR1 resulted in a marked increase of vascular density in WATs, indicating the negative role of this receptor on angiogenesis. Targeting VEGFR1 alone produced overt anti-obesity and anti-diabetic effects in obese mice. Thus, our findings provide novel mechanistic insights into the vascular role of the modulation of adipocyte metabolism and pave a new avenue for the development of drugs targeting obesity and metabolic diseases.

RESULTS

Blocking VEGFR1 augments adipose angiogenesis

To study the physiological functions of VEGFRs in adipose tissues, we chose adult C57Bl/6 mice that had not been exposed to cold or treated with any therapeutic agents. Anti-VEGFR1 and anti-VEGFR2 highly specific neutralizing antibodies were used for 10-d systemic treatment (Witte et al., 1998; Shaked et al., 2008; Kodack et al., 2012; He et al., 2015; Iwamoto et al., 2015). After the 10-d treatment, anti-VEGFR1, but not anti-VEGFR2, induced a significant angiogenic response in subWAT (Fig. 1 A). Quantitative immunoblotting further validated the increased $CD31^+$ signals (Fig. 1 B). Similarly, the VEGFR1 blockade also stimulated angiogenesis in visWAT (Fig. S1, A and B). Quantification analysis showed that total vascular density and microvascular numbers per adipocyte were significantly increased (Fig. 1 A). Consistently, double immunostaining with Ki67 and endomucin showed a significant increase in the proliferating population of ECs in the angiogenic vessels (Fig. 1 A). Additionally, the VEGFR1 blockade augmented a robust angiogenic response in BAT (Fig. S1, C and D). Despite WAT browning and BAT activation, the total adipose mass of WATs and BATs remained unchanged (Fig. S1 E).

Anti-VEGFR1–induced increases in vascularity had a functional impact on vascular perfusion in subWAT (Fig. 1 C), and the VEGFR1 blockade did increase vascular permeability (Fig. 1 C). Because VEGFR1 binds to VEGF-A, VEGF-B, and PlGF (Cao, 2009), we investigated expression levels of those angiogenic factors in anti-VEGFR1–treated subWAT. VEGF-A, but not VEGF-B or PlGF, messenger RNA (mRNA) levels were significantly increased in subWAT upon blocking VEGFR1 (Fig. 1 D), suggesting that VEGF-A might be the angiogenic driving force. To decipher the VEGF-induced angiogenic function in our experimental settings, anti-VEGFR1 and anti-VEGF were simultaneously used for a combination treatment. It was interesting that anti-VEGFR1–stimulated angiogenesis was completely ablated by the anti-VEGF treatment (Fig. 1 E), indicating VEGF was the primary driving force for enhanced angiogenesis. Together, these findings suggest that VEGF mediates the anti-VEGFR1–induced angiogenesis in WAT.

To gain further mechanistic insights of the signaling pathway of anti-VEGFR1–triggered angiogenesis, a pharmacological approach of simultaneous inhibition of VEGFR1 and VEGFR2 was used in our study. Noticeably, the combination of anti-VEGFR1 and anti-VEGFR2 completely abolished the anti-VEGFR1–induced angiogenesis and WAT browning (Fig. 1 E). These data indicate that VEGFR2 is the crucial receptor for transducing the angiogenic signal. In support of this view, anti-VEGFR1 treatment was able to induce VEGFR2 phosphorylation (Fig. 1 F). Together with the data on the combination of anti-VEGFR1 with anti-VEGF treatment, it is clear that the VEGF–VEGFR2 signaling is responsible for the angiogenic phenotype.

Anti-VEGFR1 induces WAT browning

We next studied the impact of VEGFR1 blockade on adipocytes in various adipose depots. Histological analysis showed that VEGFR1 inhibition markedly decreased the mean size of adipocytes, exhibiting dense and irregular adipocyte cell shapes (Fig. 1 G and Fig. S1, A and B). High-density, irregular cellular networks existed in the VEGFR1 blockade-treated subWAT, visWAT, and BAT (Fig. 1 G and Fig. S1, A–D). Consistently, mRNA and protein expression levels of uncoupling protein 1 (UCP1) were significantly increased in the anti-VEGFR1–treated subWAT (Fig. 1, G and H). Additionally, *Cox8b*, as a browning marker, was elevated upon anti-VEGFR1 treatment (Fig. 1 H). By contrast, UCP1 expression levels were not altered by blocking VEGFR2 (Fig. 1 G and Fig. S1, A and B). UCP1 expression was also markedly increased in anti-VEGFR1–treated visWAT (Fig. S1, A and B). Systemic anti-VEGFR1 treatment also increased UCP1 expression in BAT (Fig. S1, C and D). Smaller adipocytes and higher UCP1 expression in VEGFR1-treated WATs and BAT might suggest the activation of nonshivering thermogenesis by the VEGFR1 blockade. In contrast, anti-VEGFR1 treatment did not alter the vascularity of liver and skeletal muscle tissue, as previously described (Yang et al., 2013).

Knowing that a VEGFR1 blockade induced a browning phenotype, we measured metabolism of nonshivering thermogenesis. Notably, anti-VEGFR1 markedly enhanced the norepinephrine (NE)-induced, nonshivering thermogenesis (Fig. 1 I). By contrast, systemic treatment with an anti-VEGFR2 neutralizing antibody did not significantly affect thermogenesis-related metabolism. These data show that blocking VEGFR1 alone is able to augment a browning phenotype in WAT. Thus, VEGFR1 plays a crucial role in regulating the physiological functions of adipose tissues.

Time-course analysis of sequential events of angiogenesis and WAT browning

To address the sequence of adipose angiogenesis and adipocyte browning, we performed a time-course experiment to tightly

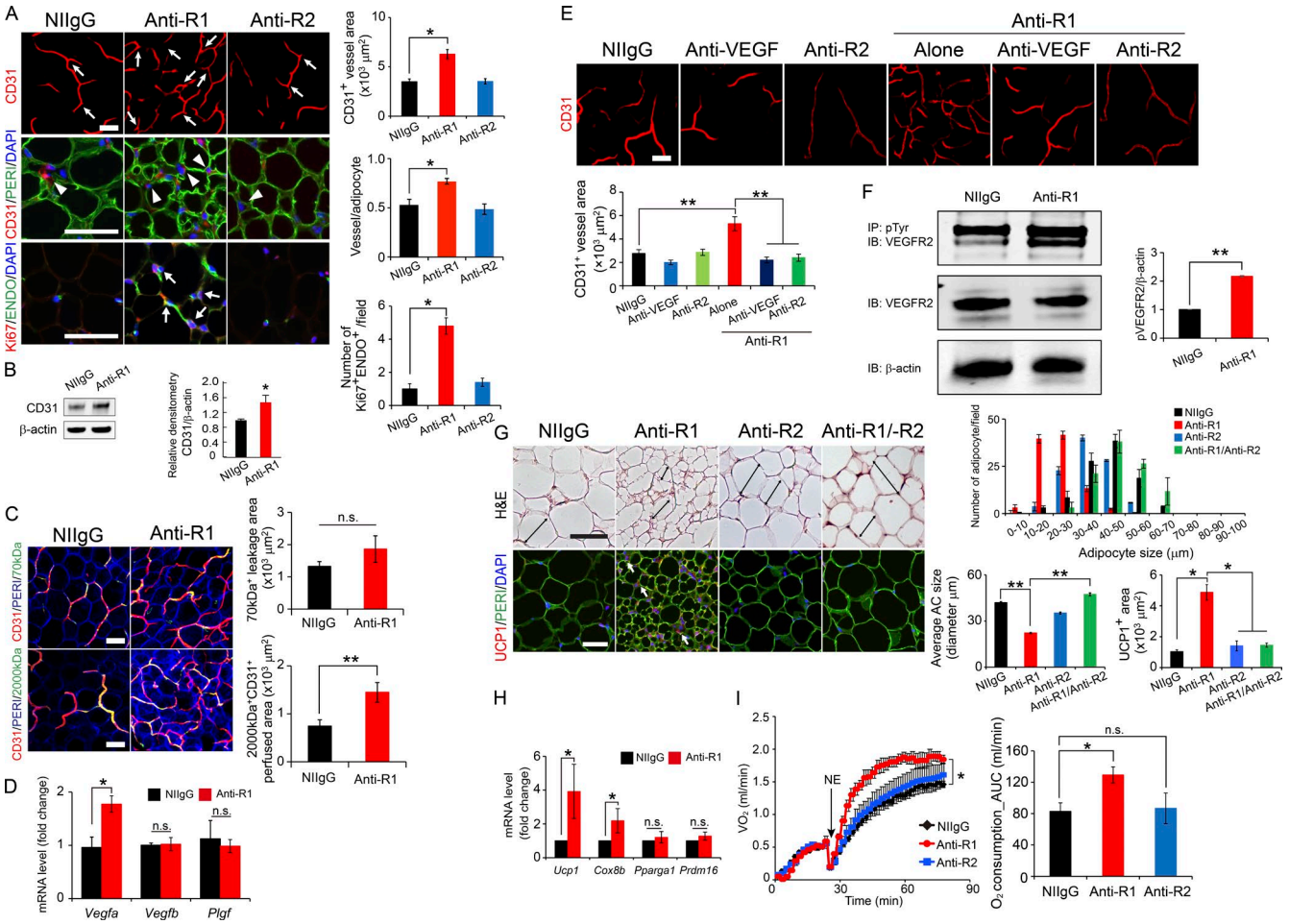

Figure 1. **Blocking VEGFR1 augments adipose angiogenesis and nonshivering thermogenesis. (A)** Immunohistological mono-, double-, or multi-color-staining of CD31$^+$ (top and middle: red) microvessels, endomucin$^+$ (bottom: green) microvessels, perilipin (PERI) and adipocytes (middle: green), and Ki67$^+$–proliferating cells of subWAT with NIIgG, anti-R1, or anti-R2 in WT C57Bl/6 mice (n = 5 mice/group). Top: Arrows point to CD31$^+$ microvessels. Middle: Arrowheads indicate cell nuclei. Bottom: Arrows indicate endomucin$^+$-Ki67$^+$-DAPI$^+$–proliferating ECs. Data were quantified from 10 randomized fields/group. Mice were euthanized 10 d after treatment of VEGFRs blockades. **(B)** Western immunoblotting analysis of CD31 of NIIgG- and anti-R1–treated subWAT in WT C57Bl/6 mice (n = 4 samples/group). β-Actin indicates loading levels. **(C)** Vascular perfusion of 2,000 kD dextran (green) and permeability of 70 kD dextran (green) were contained with CD31$^+$ vessels (red) and PERI$^+$ adipocytes (blue; n = 5 mice/group; n = 10 random fields/group for quantifications). **(D)** Quantitative analysis of *Vegfa*, *Vegfb*, and *Plgf* mRNA expression levels by qPCR (n = 6–8 samples/group). **(E)** Immunohistological staining of CD31$^+$ (red) microvessels and PERI$^+$ adipocytes of NIIgG, VEGF blockade, and anti-VEGFR2 in the presence and absence of anti-VEGFR1 treatment (n = 8 mice/group). Data were quantified (n = 10 random fields). **(F)** Western immunoblotting analysis of VEGFR2 phosphorylation of NIIgG- and anti-R1–treated subWAT in WT C57Bl/6 mice (n = 4 samples/group). β-Actin indicates loading levels. **(G)** H&E staining of adipose tissues. Double-arrowed bars indicate adipocyte diameters. PERI$^+$ (green) and UCP1$^+$ adipocytes (red) of NIIgG, anti-VEGFR1, and anti-VEGFR2 in the presence and absence of anti-VEGFR1–treated subWAT of C57Bl/6 mice (n = 5 mice/group). Arrows point to UCP1-positive signals. Data were quantified (n = 10 random fields/group). **(H)** qPCR quantification of *Ucp1*, *Cox8b*, *Pparga1*, and *Prdm16* mRNA expression levels in various agent-treated subWAT samples (n = 10 samples/group). **(I)** NE-stimulated, nonshivering thermogenesis in NIIgG-, anti-VEGFR1–, and anti-VEGFR2–treated C57Bl/6 mice (n = 5 mice/group). *, $P < 0.05$; **, $P < 0.01$; n.s. = not significant by the standard Student's t test for pair comparisons and ANOVA analysis for multiple factors. Data are presented as means ± SEM. Bars, 50 μm. Experiments were independently repeated three times.

monitor vessel growth and the WAT browning phenotype. As shown in Fig. S1, a significant increase of vascularity already occurred at day 2 after anti-VEGFR1 treatment. The vessel density continued to increase during the 10-d experimental setting (Fig. S1, F and G). Intriguingly, adipocyte sizes were not altered until day 4 (Fig. S1, F and G). Similarly, UCP1 expression levels in anti-VEGFR1-treated subWAT were barely detectable during the first 4-d period relative to those of controls (Fig. S1, F and G). At day 4, there was nearly a threefold increase of vessel density without changing adipocyte size or UCP1 expression. These data indicate that angiogenesis occurred before WAT browning in our experimental setting.

Reduction of adipocyte size and increase of UCP1 expression only occurred at day 7 (Fig. S1, F and G). Further increase of UCP1 signals was found at day 10 after anti-VEGFR1 treatment. Again, this time-course experiment demonstrates that angiogenesis occurred before WAT browning and was not dependent on the browning phenotype. Thus, angiogenesis may play predominant role in controlling the metabolic activity of adipocytes.

Genetic deletion of VEGFR1 produces WAT browning and metabolic changes

To validate the pharmacological findings, we employed genetic approaches to further investigate the VEGFR1 functions in adipose tissues. First, we used an *Flt1$^{f/f}$;Rosa26-Cre-ER^{T2}* genetic mouse strain in which the *Vegfr1* gene is deleted in adult mice by a tamoxifen-inducible system. Histological analysis of subWAT depots in *Flt1$^{f/f}$;Rosa26-Cre-ER^{T2}* mice showed the existence of smaller adipocytes and alterations in tissue architectures with high-density, irregular cellular networks 10 d after tamoxifen treatment compared with those of WT mice (Fig. 2 A). Similar to anti-VEGFR1 treatment, the subWAT of *Flt1$^{f/f}$;Rosa26-Cre-ER^{T2}* mice also contained an increased number of microvessels, which showed a significant increase of Ki67^{+} proliferating ECs (Fig. 2, A and B). Quantification of CD31 protein levels further supported the increase of vascularity in subWAT in *Flt1$^{f/f}$;Rosa26-Cre-ER^{T2}* mice versus that of control mice (Fig. 2 C). Consequently, UCP1 expression levels were also markedly elevated in the subWAT of *Flt1$^{f/f}$;Rosa26-Cre-ER^{T2}* mice relative to those of WT mice (Fig. 2, A and B). Deletion of VEGFR1 augmented a robust angiogenic response in visWAT and BAT, exhibiting a greater density of CD31^{+} microvessels (Fig. S2, A–D). Furthermore, UCP1 expression levels in the visWAT of *Flt1$^{f/f}$;Rosa26-Cre-ER^{T2}* mice were significantly higher than those of WT control mice (Fig. S2, A and B). Thus, systemic VEGFR1 deletion produced a functional impact on both WATs and BATs. Again, during this short experimentation period, the total mass of browning WAT and BAT was not significantly altered in *Flt1$^{f/f}$;Rosa26-Cre-ER^{T2}* mice relative to control mice (Fig. S2 E). The nonshivering thermogenesis was significantly increased in *Flt1$^{f/f}$;Rosa26-Cre-ER^{T2}* mice (Fig. 2 D). Taken together, genetic ablation of VEGFR1 validates the physiological function of this receptor in modulation of adipose metabolism.

Endothelial deletion of VEGFR1 induces WAT browning

Because blood vessel ECs are not the only VEGFR1-expressing cell type (Shibuya, 2006, 2014), we investigated the impact of EC VEGFR1 deletion on adipose angiogenesis and WAT browning. We generated two endothelial cell–specific VEGFR1-deletion mouse strains, *Flt1$^{f/f}$;Tie2-Cre-ER^{T2}* and *Flt1$^{f/f}$;Cdh5-Cre-ER^{T2}*. A *Tie2* promoter-inducible *Cre* mouse strain was crossed with *Flt1$^{f/f}$* mice to generate the *Flt1$^{f/f}$;Tie2-Cre-ER^{T2}* stain. The KO efficiency of *Vegfr1* mRNA was sufficiently high 8 d after tamoxifen treatment (Fig. S3 A). *Flt1$^{f/f}$;Tie2-Cre-ER^{T2}* mice showed induction of angiogenesis and activation of a browning phenotype in subWAT 8 d after tamoxifen treatment (Fig. 3, A–C). Again, UCP1 expression levels of subWAT were markedly elevated in *Flt1$^{f/f}$;Tie2-Cre-ER^{T2}* mice relative to controls (Fig. 3, A–D). Moreover, the visWAT of *Flt1$^{f/f}$;Tie2-Cre-ER^{T2}* mice also contained an increased number of microvessels and exhibited a browning phenotype without affecting the total adipose mass (Fig. S3, B–D).

Because *Tie2* expression is not restricted to vascular ECs (Welford et al., 2011), we created another genetic strain of mice carrying a specific deletion of VEGFR1 in ECs using the cadherin promoter-inducible *Cre* system. *Flt1$^{f/f}$;Cdh5-Cre-ER^{T2}* mice showed effective deletion of VEGFR1 on ECs in adipose tissue 8 d after tamoxifen treatment (Fig. S4 A). *Flt1$^{f/f}$;Cdh5-Cre-ER^{T2}* mice did not have altered body weight or body mass index (BMI; Fig. S4 B) within the experimental duration. The total adipose mass of WAT and BAT was not significantly changed in *Flt1$^{f/f}$;Cdh5-Cre-ER^{T2}* mice versus that of control mice (Fig. S4 C). In *Flt1$^{f/f}$;Cdh5-Cre-ER^{T2}* mice, subWAT showed a marked increase in angiogenesis and a browning phenotype (Fig. 4, A–D). Smaller WAT adipocytes with high-density cellular contents showing high levels of UCP1 expression only existed in *Flt1$^{f/f}$;Cdh5-Cre-ER^{T2}* mice, not in WT control mice (Fig. 4, A–D). Likewise, visWAT exhibited similar increases of microvessel density and the browning phenotype (Fig. S4, D and E). Both microvessel density and UCP1 expression levels were also increased in the BAT of *Flt1$^{f/f}$;Cdh5-Cre-ER^{T2}* mice (Fig. S4, F and G). No vascular changes were seen in liver and skeletal muscle tissues. Consequently, *Flt1$^{f/f}$;Cdh5-Cre-ER^{T2}* mice resulted in elevated global metabolisms (Fig. 4 E). There were no differences in locomotor activity between WT and *Flt1$^{f/f}$;Cdh5-Cre-ER^{T2}* mice. These results indicate the physiological functions of VEGFR1 in modulating physiological metabolisms. We further investigated the possibility of a combination treatment with the deletion of VEGFR1 and WAT browning agents, such as catecholamine and cold, to produce a combination treatment with greater effects on browning. We employed a β3 adrenoceptor agonist, CL316,243 (CL), treatment to *Flt1$^{f/f}$;Cdh5-Cre-ER^{T2}* mice. Deletion of VEGFR1 further augmented CL-induced angiogenesis and browning in subWAT compared with CL-treated WT control mice (Fig. 4, F and G). It was plausible that macrophages, especially the alternatively activated macrophages (M2) macrophage population might contribute to WAT browning, as shown in other experimental settings (Nguyen et al., 2011; Shan et al., 2017). To investigate this possibility, we measured the total number of macrophages and M2 macrophage polarization. As shown Fig. S4, the total number of macrophages by immunohistological staining with macrophage-specific marker and the M2 macrophage subpopulation by qPCR analysis remained unchanged. These findings demonstrate that VEGFR1 in vascular ECs, but not in other cells, plays crucial roles in the modulation of adipose tissue metabolism.

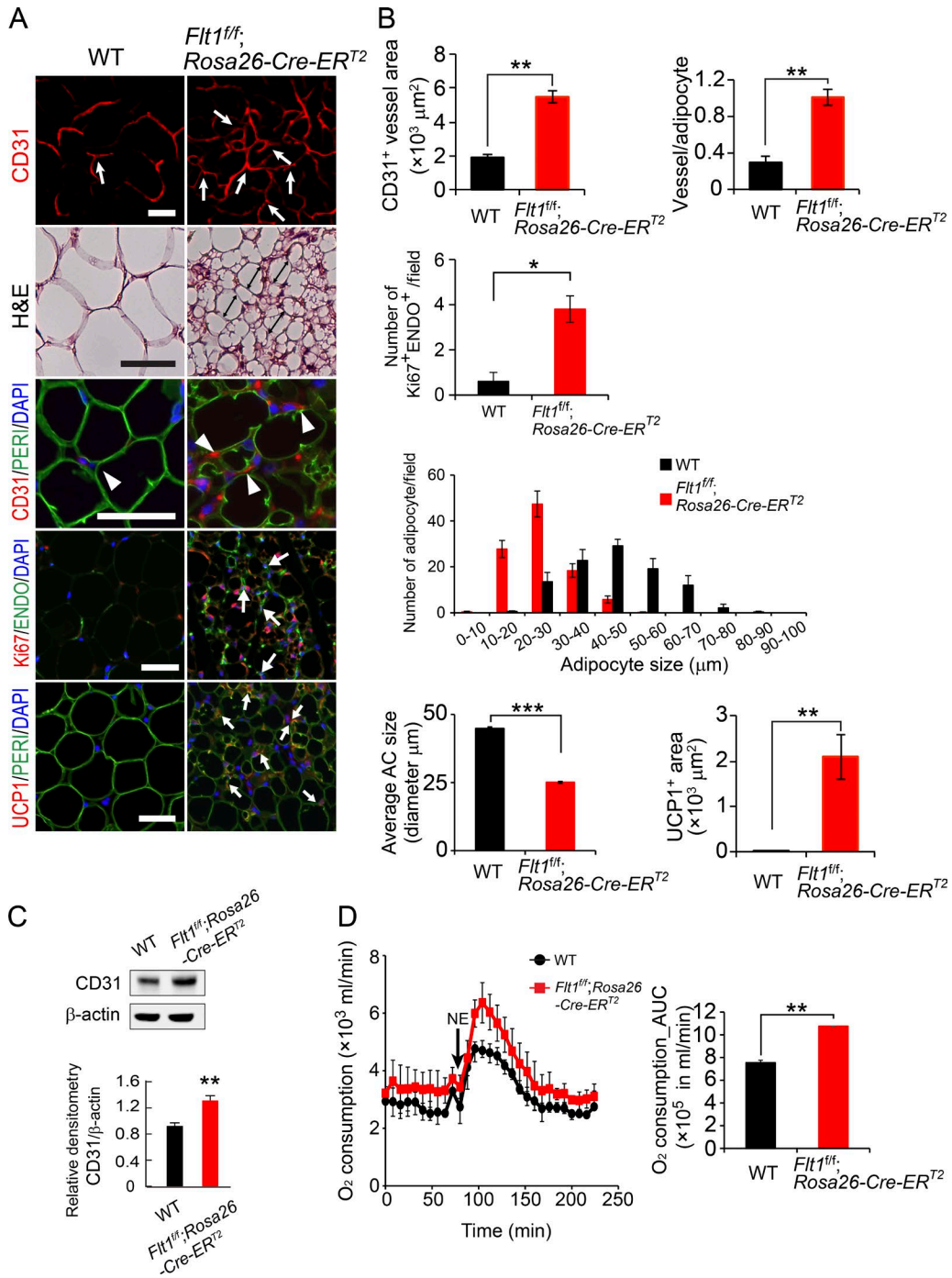

Figure 2. **Genetic deletion of VEGFR1 promotes WAT browning and metabolism. (A)** Immunohistological mono- or multicolor-staining of CD31$^+$ (top and middle: red) microvessels, PERI$^+$ adipocytes (green), UCP1$^+$ adipocytes, and Ki67$^+$-proliferating cells of subWAT in WT littermate control and *Flt1$^{f/f}$;Rosa26-Cre-ER^{T2}* mice (n = 5 mice/group). Top and middle: Arrows show CD31$^+$ signals. Arrowheads in middle panels show CD31-positive signals. Doubled-headed arrows show adipocyte size. Bottom: Arrows show UCP1$^+$ signals. **(B)** Data were quantified (n = 10 random fields/group; n = 5 mice/group). **(C)** Western immunoblotting analysis of subWAT CD31 of WT littermate control and *Flt1$^{f/f}$;Rosa26-Cre-ER^{T2}* mice (n = 4 samples/group). β-Actin indicates loading levels. **(D)** NE-stimulated, nonshivering thermogenesis of WT littermate control and *Flt1$^{f/f}$;Rosa26-Cre-ER^{T2}* mice (n = 5 mice/group). Mice were sacrificed 10 d after tamoxifen treatment. *, P < 0.05; **, P < 0.01; ***, P < 0.001 by the standard Student's t test for pair comparisons. Bars, 50 μm. Data are presented as means ± SEM. Experiments were independently repeated three times.

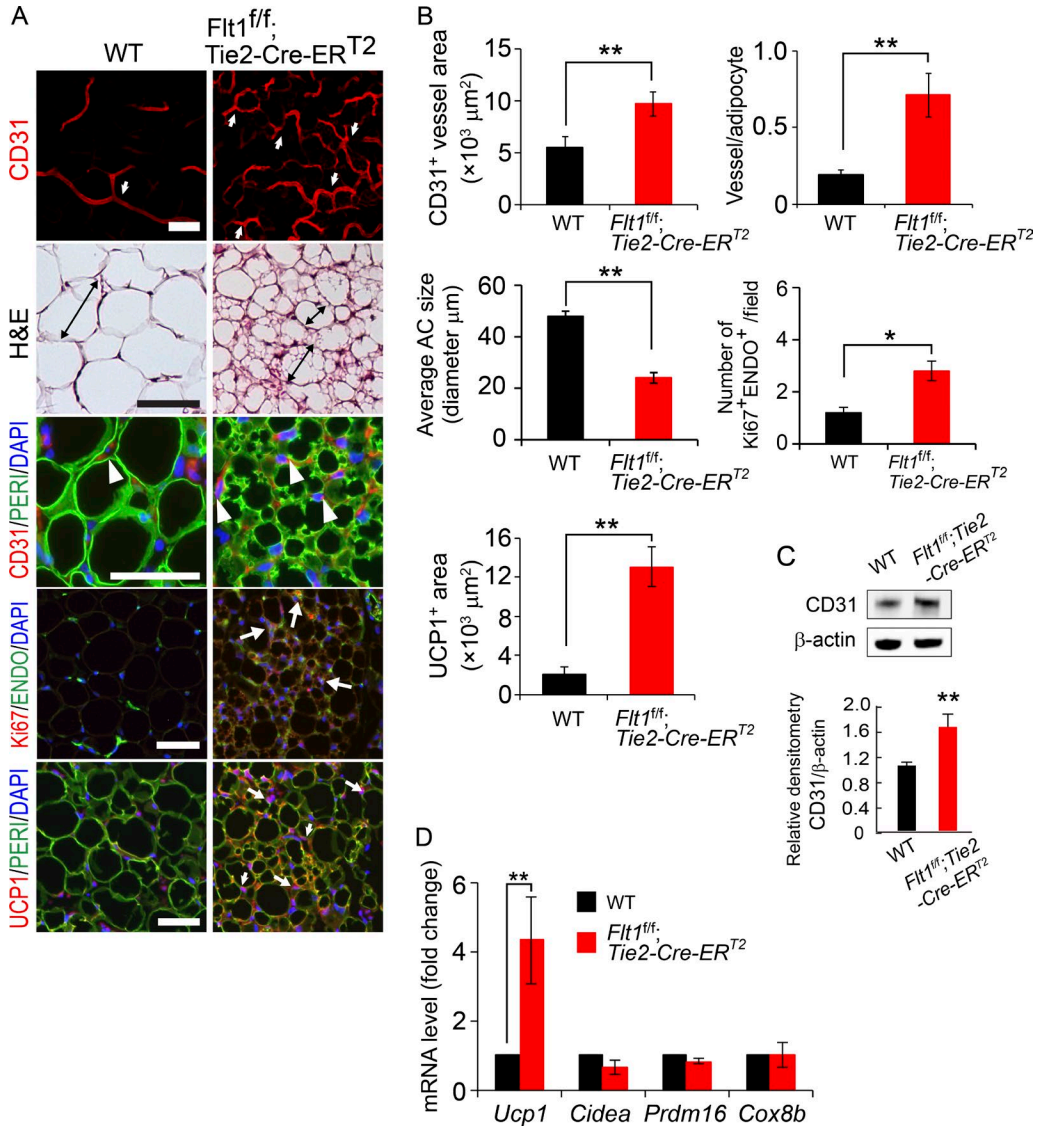

Figure 3. **Endothelial deletion of VEGFR1 stimulates WAT browning. (A)** Immunohistological mono- or multicolor-staining of CD31$^+$ (top and middle: red) microvessels, PERI$^+$ adipocytes (green), UCP1$^+$ adipocytes, and Ki67$^+$-proliferating cells of subWAT in WT littermate control and *Flt1$^{f/f}$;Tie2-Cre-ER^{T2}* mice (n = 5 mice/group). Top and middle: Arrows show CD31$^+$ signals. Arrowheads in middle panels show CD31-positive signals. Doubled-headed arrows show adipocyte size. Bottom: Arrows show UCP1$^+$ signals. **(B)** Immunohistochemical data were quantified from 10 randomized fields/group. **(C)** Western immunoblotting analysis of subWAT CD31 of WT littermate control and *Flt1$^{f/f}$;Tie2-Cre-ER^{T2}* mice (n = 4 samples/group). β-Actin indicates loading levels. **(D)** qPCR analysis of mRNA expression levels of browning markers in WT littermate control and *Flt1$^{f/f}$;Tie2-Cre-ER^{T2}* subWAT (n = 6 samples/group). Mice were sacrificed 8 d after tamoxifen treatment. *, P < 0.05; **, P < 0.01 by the standard Student's t test for pair comparisons. Bars, 50 μm. Data are presented as means ± SEM. Experiments were independently repeated twice.

Deletion of endothelial VEGFR1 ameliorates obesity and metabolic dysfunctions

Next, we employed high fat diet (HFD) to induce obesity in *Flt1$^{f/f}$;Cdh5-Cre-ER^{T2}* mice. It was interesting that *Flt1$^{f/f}$;Cdh5-Cre-ER^{T2}* mice showed an overt lean phenotype compared with WT control mice (Fig. 5 A). HFD-induced body weight and BMI gains were markedly reduced relative to controls (Fig. 5, B and C). However, food intake remained the same in *Flt1$^{f/f}$;Cdh5-Cre-ER^{T2}* and WT mice (Fig. 5 C), indicating no impact on food intake after removal of endothelial VEGFR1. Analysis of body composition demonstrated a significant reduction of subWAT, visWAT, and even BAT masses (Fig. 5 D). *Flt1$^{f/f}$;Cdh5-Cre-ER^{T2}* mice demonstrated marked improvement in lipid profile by decreasing blood levels of free fatty acid (FFA), glycerol, cholesterol, triglyceride (TG), glucose, and insulin (Fig. 5 E). These results show that elimination of endothelial VEGFR1 significantly ameliorated dysfunctions of lipid and glucose metabolism.

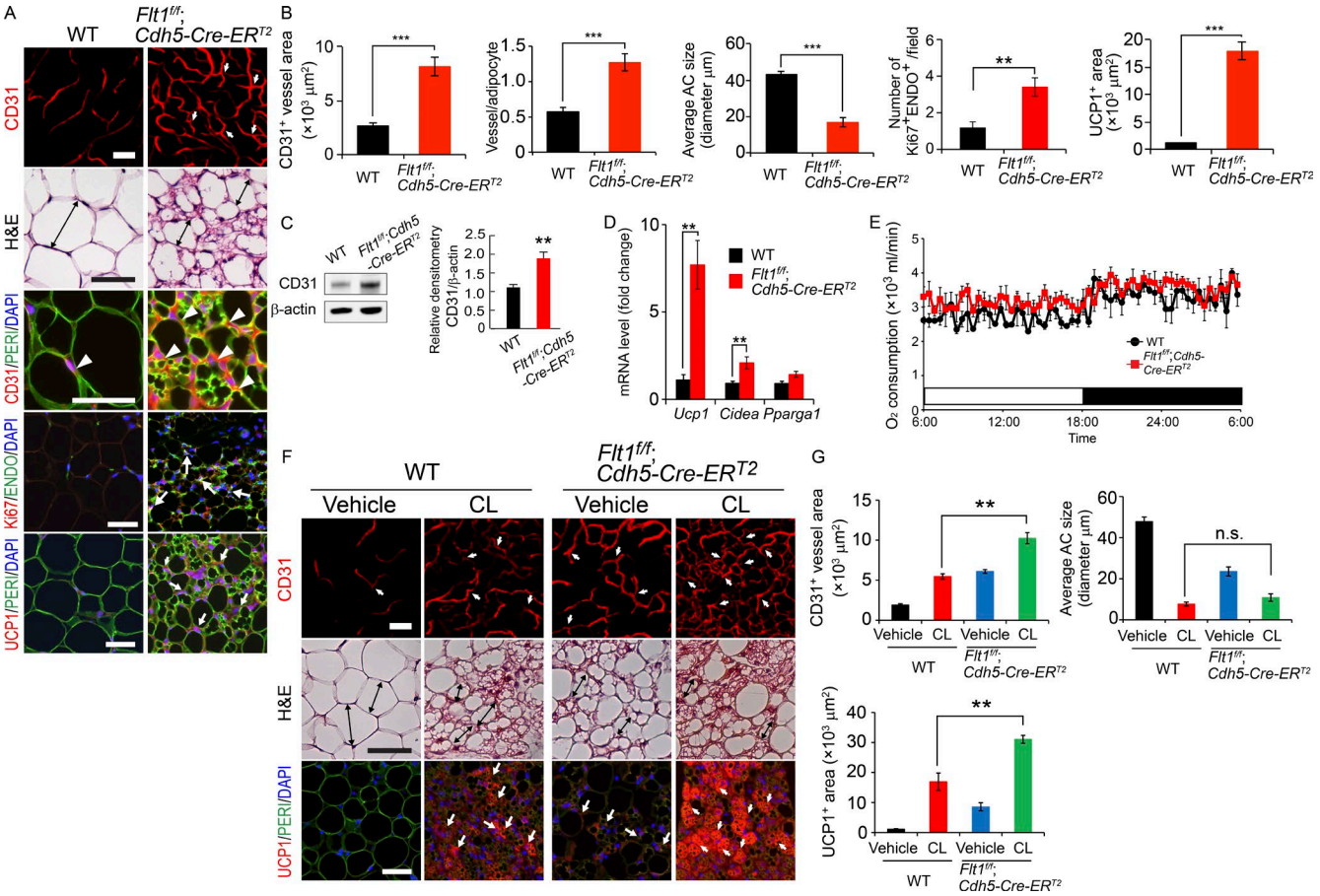

Figure 4. **Endothelial deletion of VEGFR1 stimulates WAT browning and metabolism. (A)** Immunohistological mono- or multicolor-staining of CD31$^+$ (top and middle: red) microvessels, PERI$^+$ adipocytes (green), UCP1$^+$ adipocytes and Ki67$^+$-proliferating cells of subWAT in WT and *Flt1$^{f/f}$;Cdh5-Cre-ER^{T2}* mice (n = 5 mice/group). Top and middle: Arrows show CD31$^+$ signals. Arrowheads in middle panels show CD31-positive signals. Doubled-headed arrows show adipocyte size. Bottom: Arrows show UCP1$^+$ signals. **(B)** Immunohistochemical data were quantified from 10 randomized fields/group. **(C)** Western immunoblotting analysis of subWAT CD31 of WT littermate control and *Flt1$^{f/f}$;Cdh5-Cre-ER^{T2}* mice (n = 4 samples/group). β-Actin indicates loading levels. **(D)** qPCR analysis of mRNA expression levels of browning markers in WT and *Flt1$^{f/f}$;Cdh5-Cre-ER^{T2}* subWAT (n = 6 samples/group). **(E)** O_2 consumption of WT littermate control and *Flt1$^{f/f}$;Cdh5-Cre-ER^{T2}* mice (n = 5 mice/group). White and black bars show day and night, respectively. **(F)** Immunohistological mono- or multicolor-staining of CD31$^+$ (top: red) microvessels, H&E adipocyte morphology, PERI$^+$ adipocytes (bottom: green), and UCP1$^+$ adipocytes (bottom: red) of vehicle- and CL-treated subWAT in WT and *Flt1$^{f/f}$;Cdh5-Cre-ER^{T2}* mice (n = 4 mice/group). Arrows in top panels show CD31-positive signals; arrows in bottom panels show UCP1-positive signals. Doubled-headed arrows show adipocyte size. **(G)** Immunohistochemical data were quantified from eight randomized fields/group. Mice were sacrificed 8 d after tamoxifen treatment. **, $P < 0.01$; ***, $P < 0.001$ by the standard Student's t test for pair comparisons. Bars, 50 μm. Data are presented as means ± SEM. Experiments were independently repeated twice.

In support of this notion, *Flt1$^{f/f}$;Cdh5-Cre-ER^{T2}* mice showed considerable improvement in glucose clearance and insulin tolerance relative to HFD-fed control animals (Fig. 5, F and G), indicating that targeting of this receptor provides an opportunity for treatment of type 2 diabetes. Notably, EC deletion of VEGFR1 showed obvious decreases of lipid deposition in hepatocytes (Fig. 5 H), suggesting the therapeutic possibility of fatty liver by targeting VEGFR1. Along with improving lipid profile, nonshivering thermogenesis in *Flt1$^{f/f}$;Cdh5-Cre-ER^{T2}* mice was significantly higher than it was in control mice (Fig. 5 I). These findings show that ablation of VEGFR1 in ECs markedly improved metabolic dysfunctions.

In further support, *Flt1$^{f/f}$;Tie2-Cre-ER^{T2}* mice also exhibited suppression of HFD-induced gains in body weight and BMI, without affecting food intake in the diet-induced obesity model (Fig. S5, A and B). Fat mass was also significantly decreased in *Flt1$^{f/f}$;Tie2-Cre-ER^{T2}* mice relative to that of control mice (Fig. S5 C). Glucose and insulin tolerance tests showed obvious improvements in glucose clearance and insulin sensitivity in the HFD-fed, obese mice (Fig. S5, D and E). Again, HFD-induced hepatic steatosis was significantly suppressed relative to that of control mice (Fig. S5 F). Taken together, in two genetic models, we show that deletion of VEGFR1 in ECs produced significant improvements in body weight reduction without affecting food intake, blood lipid profile, insulin sensi-

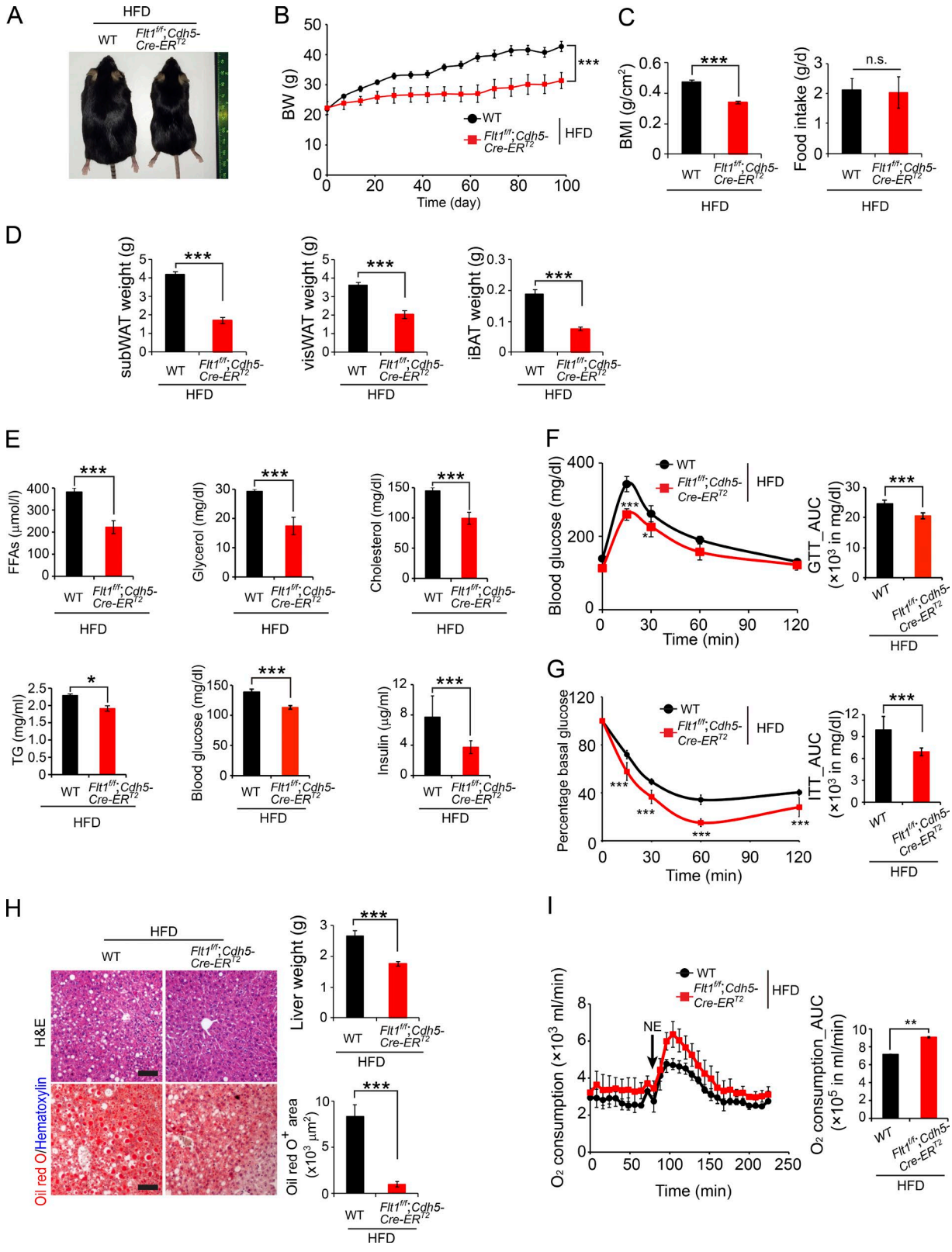

Figure 5. **Genetic deletion of endothelial VEGFR1 shows antiobesity and metabolic improvement. (A)** Representative mouse pictures of HFD-fed WT littermate control and *Flt1*$^{f/f}$*;Cdh5-Cre-ER*^{T2} mice (n = 6 mice/group). WT littermate control and *Flt1*$^{f/f}$*;Cdh5-Cre-ER*^{T2} female mice at 8 wk old were fed with HFD for 12 wk. **(B)** Body weights (BWs) of HFD-fed WT littermate control and *Flt1*$^{f/f}$*;Cdh5-Cre-ER*^{T2} mice (n = 6 mice/group). **(C)** BMI and food intake of

tivity, or hepatic steatosis. The antiobesity and antidiabetic effects in these genetic mice are likely due to the reduction of adipose masses solely without affecting other tissue masses.

Deletion of VEGFR1 in adipocytes and myeloid cells produces no functional effects

Because VEGFR1 is expressed in many cell types, including adipocytes and myeloid cells (Kerber et al., 2008; Cao, 2009; Beck et al., 2010; Liu et al., 2012), blocking VEGFR1 might have autonomous effects on these cells, which eventually affects the global metabolism. Although UCP1 expression in differentiated mature adipocytes was unchanged by anti-VEGFR1 (Fig. 6 A), we generated two genetic mouse strains, *Flt1$^{f/f}$;Adipoq-Cre* and *Flt1$^{f/f}$;LysM-Cre*, in order to rule out these possibilities. VEGFR1 deletion from either adipocytes or myeloid cells was acheived by crossing *Flt1$^{f/f}$* mice with *Adipoq-Cre* and *LysM-Cre* mice, respectively. However, adipose angiogenesis, adipocyte morphology, and UCP1 expression levels remained unchanged in *Flt1$^{f/f}$;Adipoq-Cre* mice relative to WT control mice (Fig. 6, B and C).

To exclude the involvement of inflammatory cells that often express VEGFR1 in our experimental settings, we generated a *Flt1$^{f/f}$;LysM-Cre* genetic mouse strain carrying a specific deletion of VEGFR1 in monocytes/macrophages and CD11b^{+} splenic dendritic cells, neutrophils, and some B cells (Sander et al., 2008; Gordts et al., 2014; Howangyin et al., 2016). Despite sufficient deletion of VEGFR1 in CD11b^{+} cells in *Flt1$^{f/f}$;LysM-Cre* mice, no alteration in adipose angiogenesis, adipocyte morphological phenotypes, and UCP1 expression were observed compared with those of WT littermate control mice (Fig. 6, D–F). In addition, adipocyte and myeloid deletion of VEGFR1 did not significantly alter macrophage populations relative to their respective controls (Fig. S5, G and H). Furthermore, cytokines inducing browning—IL-4, -6, and -10—were unchanged in pharmacological inhibition and genetic deletion of endothelial VEGFR1 experimental models (Fig. S5, I–K). These data exclude the potential autonomous effect of VEGFR1 on non-ECs.

DISCUSSION

Increasing evidence shows that blood vessels in adipose tissues play an important role in controlling adipose tissue functions (Yang et al., 2013). WAT browning and activation of BAT concomitantly switch to an angiogenic phenotype as adipocytes undergo thermogenic reprogramming (Xue et al., 2009; Seki et al., 2016). Several key questions around these two concomitant processes need mechanistic efforts to gain insights. These include the following: (a) which of these two processes occurs first during browning; (b) which process plays a predominant role in controlling thermogenesis; and (c) would intervention of one process affect the other? It was originally thought that hypervascularization in the metabolically active beige WAT and BAT provided fuel for energy consumption and metabolic changes in adipocytes would be the initial trigger for angiogenesis (Asano et al., 1997). However, our previous findings have changed this view because genetic deletion of UCP1 does not affect cold-induced angiogenesis in browning WAT and BAT (Xue et al., 2009; Dong et al., 2013). Thus, adipocyte-derived metabolites cannot be the primary driving force for switching to the angiogenic phenotype.

The angiogenic program in browning WAT and BAT is tightly controlled by a metabolic-independent mechanism. Our recent studies show that VEGF is the key factor responsible for the angiogenic switch in browning WAT under cold exposure (Xue et al., 2009; Dong et al., 2013). Blocking of VEGF or VEGFR2 signaling completely inhibits adipose angiogenesis (Xue et al., 2009; Honek et al., 2014), demonstrating the crucial role of VEGF–VEGFR2 signaling in cold-induced angiogenesis. Moreover, genetic deletion of VEGFR2 in ECs also partly prevents angiogenesis in browning adipose tissues (Seki et al., 2016). Interestingly, blocking the VEGF–VEGFR2 signaling pathway significantly affects CL-induced WAT adipocyte browning. Because VEGFR2 is exclusively expressed in blood vessel ECs, but not in adipocytes, these genetic and pharmacological loss-of-function data demonstrate the existence of a paracrine loop in which ECs control adipocyte functions.

Our time-course experimental data showed that angiogenesis was initiated several days before the browning of WAT. This intriguing finding supports the fact that angiogenesis occurs independent of adipocyte metabolic status. These data also provide compelling evidence to support our view of the primary function of adipose vasculature in regulating adipocyte functions. Thus, vascular changes occur before adipocyte changes.

Physiological functions of VEGF and its receptor VEGFR1 remain largely uncharacterized (Cao, 2009). Although VEGFR1 may transduce positive signals for angiogenesis and other vascular functions, other studies suggest the decoyed role of this receptor in the modula-

HFD-fed WT littermate control and *Flt1$^{f/f}$;Cdh5-Cre-ER^{T2}* mice (n = 6 mice/group). **(D)** Weights of various adipose depots of HFD-fed WT littermate control and *Flt1$^{f/f}$;Cdh5-Cre-ER^{T2}* mice (n = 6 samples/group). **(E)** Blood levels of FFA, glycerol, cholesterol, TG, fasting serum levels of glucose, and serum levels of insulin in HFD-fed WT littermate control and *Flt1$^{f/f}$;Cdh5-Cre-ER^{T2}* mice (n = 6 samples/group). **(F)** Glucose tolerance test (GTT) of HFD-fed WT littermate control and *Flt1$^{f/f}$;Cdh5-Cre-ER^{T2}* mice (n = 10 mice/group). **(G)** Insulin tolerance test (ITT) of HFD-fed WT and *Flt1$^{f/f}$;Cdh5-Cre-ER^{T2}* mice (n = 10 mice/group). **(H)** Liver histology: liver weight and quantification of Oil Red O staining (n = 6 samples/group) of HFD-fed WT littermate control and *Flt1$^{f/f}$;Cdh5-Cre-ER^{T2}* mice. **(I)** NE-stimulated, nonshivering thermogenesis in HFD-fed WT littermate control and *Flt1$^{f/f}$;Cdh5-Cre-ER^{T2}* mice (n = 5 mice/group) and O_2 consumption data presented as AUC (n = 5 mice/group). *, $P < 0.05$; **, $P < 0.01$; ***, $P < 0.001$; n.s. = not significant by the standard Student's t test for pair comparisons and ANOVA analysis for multiple factors. Bars, 50 µm. Data are presented as means ± SEM. Experiments were independently repeated twice.

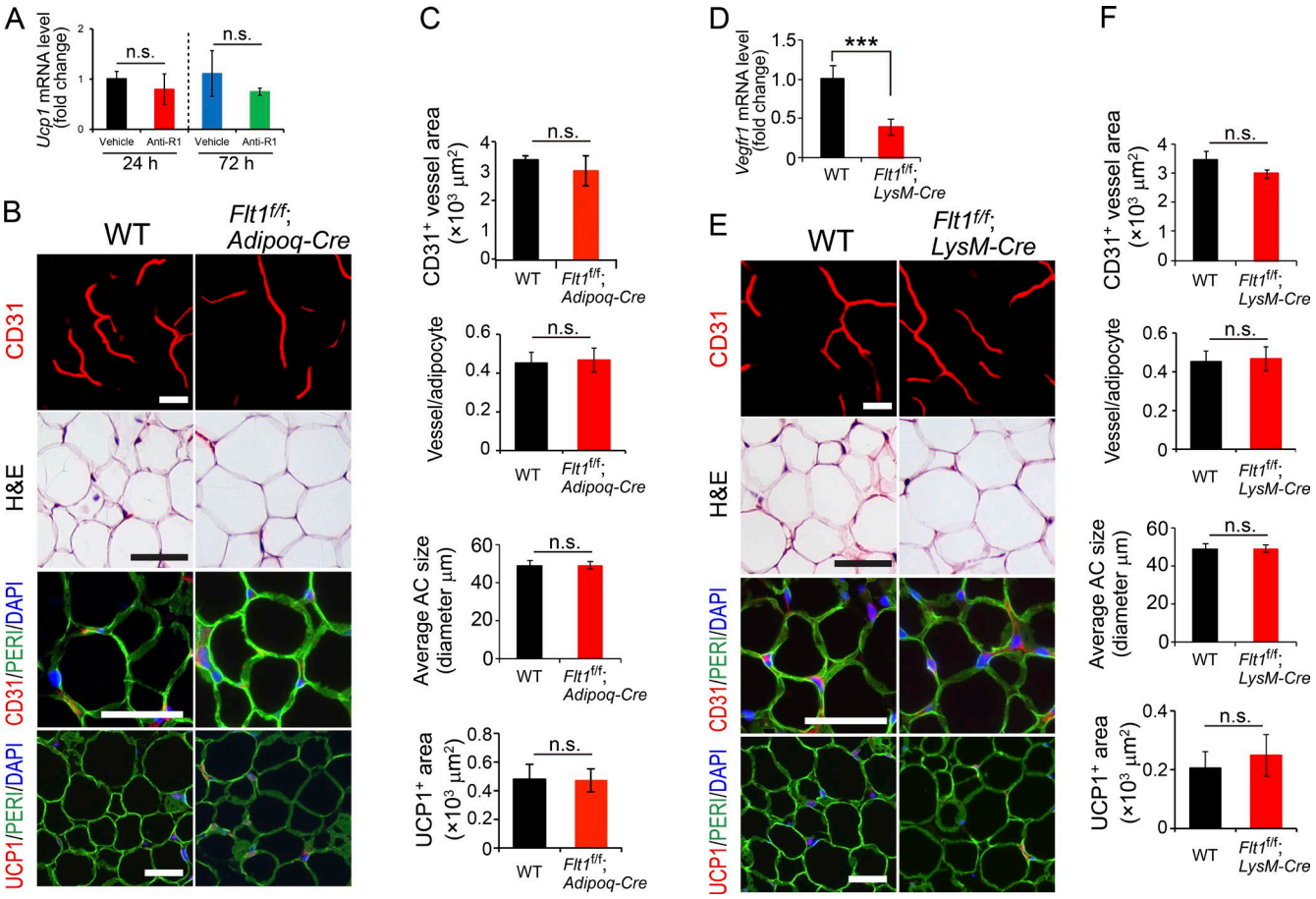

Figure 6. **Nonautonomous effects of anti-VEGFR1–triggered WAT browning. (A)** qPCR analysis of *Ucp1* mRNA expression in the anti-VEGFR1–treated 3T3442A mature adipocytes (n = 6 samples/group). **(B)** Histological images of CD31$^+$ microvessels, H&E adipocyte morphology, PERI$^+$ adipocytes, and UCP1$^+$ adipocytes from subWAT in WT littermate control and *Flt1$^{f/f}$;Adipoq-Cre* mice (n = 5 mice/group). **(C)** Quantification of vessel density, adipocyte sizes, and UCP1 expression (n = 10 samples/group). **(D)** *Vegfr1* mRNA expression levels of the CD11b$^+$ cell fraction of subWAT from WT littermate control and *Flt1$^{f/f}$;LysM-Cre* mice (n = 6 samples/group). **(E)** Histological images of CD31$^+$ microvessels, H&E adipocyte morphology, PERI$^+$ staining, and UCP1$^+$ adipocytes of subWAT from WT littermate control and *Flt1$^{f/f}$;LysM-Cre* mice (n = 5 mice/group). **(F)** Data were quantified from 10 random fields. ***, P < 0.001; n.s. = not significant by the standard Student's t test for pair comparisons. Bars, 50 µm. Data are presented as means ± SEM. Experiments were independently repeated twice.

tion of VEGF functions (Cao, 2009). We show the suppressive role of VEGFR1 in WAT vascular homeostasis under physiological functions. Surprisingly, inhibition of VEGFR1 alone, without any exogenous stimulation with growth factors, augmented a robust angiogenic response. Interestingly, anti-VEGFR1 also significantly increased VEGF expression, which could be the driving force for inducing browning. Why would anti-VEGFR1 treatment increase VEGF expression? At the time of writing, the exact mechanism underlying the anti-VEGFR1–triggered VEGF expression is unknown. However, we speculate that browning adipocytes might produce higher levels of VEGF than the quiescent white adipocytes, as seen in other experimental settings (Seki et al., 2016). Once the browning phenotype is initiated in the adipose tissue, VEGF production might be elevated.

Our findings are in sharp contrast to a recent study showing the positive role of VEGF-B–VEGFR1 signaling in the modulation of adipose metabolism (Robciuc et al., 2016). Our data differ from their findings: (a) our experimental settings were under physiological conditions without introducing any exogenous factors, whereas the study by Robciuc et al. (2016) used a VEGF-B–expressing, adeno-associated vector; (b) because VEGFR1 binds to both VEGF-B and PlGF, it is highly plausible that PlGF also plays an important physiological role in adipose metabolism. Pharmacological and genetic ablation of VEGFR1 would block the physiological functions of both factors. Thus, our approaches address broader physiological functions that were not limited to VEGF-B; (c) the previous study cannot exclude the autonomous role of VEGF-B–VEGFR1 on adipocytes and other nonvascular cells, whereas our genetic

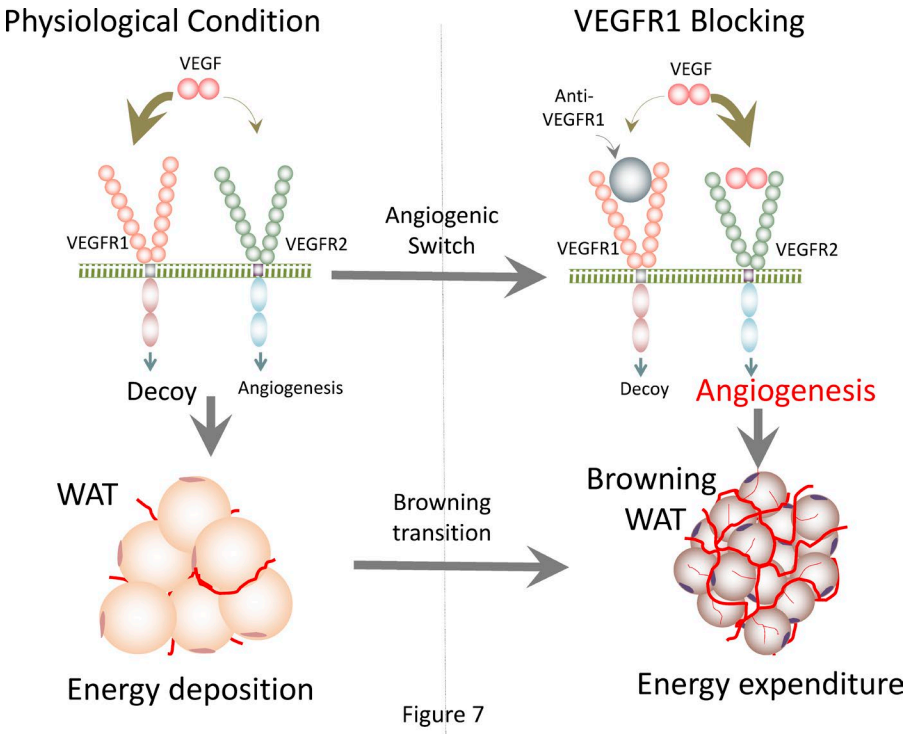

Figure 7

Figure 7. **Mechanism underlying VEGFR1 blocking–triggered WAT browning.** Under physiologically ambient temperatures, WATs remain metabolically quiescent and store excessive energy. Microvascular density in metabolically quiescent WAT is relatively low. Because VEGF preferentially binds to VEGFR1 with a 10-fold higher affinity than VEGFR2, a limited number of VEGF ligands would preferentially bind to VEGFR1, which acts as a decoy receptor. However, blocking VEGFR1 would reinforce VEGF binding to VEGFR2, which transduces angiogenic signals. It is known that angiogenic ECs produce paracrine factors to convey a browning phenotype of WAT. Browning adipocytes consume excessive energy through activation of a nonshivering thermogenesis mechanism.

models, with specific ablation of EC VEGFR1, produced an overt browning phenotype; and (d) VEGFR1 is also known to be expressed in non-ECs, including adipocytes and myeloid cells (Cao, 2009; Liu et al., 2012). Thus, it is plausible the VEGFR1$^+$ non-ECs might play a crucial role in regulating adipose function. The authors of the previous study investigated only the role of endothelial VEGFR1 in regulating adipocyte function. We used two additional genetic mouse models to address this important issue. Specific genetic deletion of VEGFR1 in adipocyte and myeloid did not produce overt phenotypes, hence, excluding the non-EC VEGFR1 function in adipose metabolism.

Browning of WAT by genetic deletion of endothelial VEGFR1 establishes a paracrine regulatory loop in which ECs control adipocyte metabolism (Fig. 7). Pharmacological and genetic ablation of VEGFR1 may switch VEGF to VEGFR2 signaling and thereby enhance the VEGFR2-mediated angiogenesis. Indeed, dual blocking VEGFR1 and VEGF by a combination of VEGF and VEGFR1 blockades completely prevents an angiogenic phenotype in WAT. Similarly, dual inhibition of VEGFR1 and VEGFR2 completely blocked anti-VEGFR1–induced angiogenesis and WAT browning. These data suggest that VEGF, but not other VEGFR1 ligands, is the primary driving force in VEGFR1 inhibition-triggered angiogenesis. VEGF-dependent angiogenesis in the absence of VEGFR1 indicates that VEGFR2 transduces active signals. The functional switch from negative VEGFR1 to positive VEGFR2 without excessive VEGF suggests the existence of an extremely sensitive balance between these two receptors. At the molecular level, we also show that anti-VEGFR1 treatment alone is able to induce VEGFR2 phosphorylation in WAT. Under physiological nonbrowning conditions, VEGFR1 predominates its functions by preventing vessel growth. In fact, VEGF binds to VEGFR1 with 10-fold higher affinity than it does to VEGFR2 (Hiratsuka et al., 2001). When VEGF is expressed at a modest level, it preferentially binds to VEGFR1, not VEGFR2. All these data support the general view that VEGFR1 serves as a negative regulator of adipose angiogenesis. Thus, adipose vasculatures remain quiescent under physiological conditions. Blocking VEGFR1 redirects VEGF to interact with VEGFR2, which induces angiogenesis. This is a tightly regulated system, and the expression level of each ligand and receptor should be optimal, otherwise creating situations of too few or too many microvessels in the fat tissues. Optimal expression of VEGF is crucial during embryonic development, as demonstrated by haploinsufficiency being lethal in mice carrying only one functional VEGF allele i.e., lowering the amount of VEGF to half (Carmeliet et al., 1996; Ferrara et al., 1996). Along with this observation, our recent studies demonstrated the existence of a paracrine regulatory mechanism in which angiogenic ECs produce platelet-derived growth factor (PDGF)-CC to control preadipocyte differentiation into beige adipocytes (Seki et al., 2016). It appears that the VEGF–EC–PDGF–preadipocyte axis operates WAT browning. Thus, blocking either VEGF–VEGFR2 signaling or PDGF-CC–PDGFRα signaling could effectively inhibit browning.

Ablation of VEGFR1 in ECs also markedly inhibits obesity in HFD-fed mice by reducing WAT masses. Strikingly, mice lacking VEGFR1 do not seem to develop liver

steatosis and show improvement in insulin sensitivity and in their blood lipid profiles. Based on these findings, we propose that pharmacological blocking of VEGFR1 provides a novel therapeutic approach for treatment of obesity, liver steatosis, and diabetes. Given clinically available anti-VEGF and anti-VEGFR2 drugs for treatment of cancer and eye disease, development of an anti-VEGFR1–neutralizing antibody for treatment of metabolic disease would be a straightforward and feasible therapeutic approach. Another interesting notion is that ablation of VEGFR1 could further augment other agent-induced browning phenotypes of WAT. In this study, we showed that deletion of VEGFR1 further augmented β3 adrenoceptor CL-316,243-induced angiogenesis and browning. These findings would suggest that a combination of anti-VEGFR1 agents with the known WAT browning agents would produce greater effects on nonshivering thermogenesis and ultimately provide metabolic improvement in the treatment of type 2 diabetes and other metabolic diseases.

MATERIALS AND METHODS

Animals

C57Bl/6 mice were obtained from the breeding unit at the Department of Microbiology, Tumor and Cell Biology, Karolinska Institute (Stockholm, Sweden). For all experiments, mice were randomly divided into groups. All mouse studies were approved by the Northern Stockholm Experimental Animal Ethical Committee.

Antibodies and reagents

Dexamethasone (DEX), insulin, 3-isobutyl-1-methylxanthine (IBMX), isoproterenol, and tamoxifen were purchased from the Sigma-Aldrich. Primer sequences for all PCR and quantitative PCR (qPCR) experiments are listed in Table S1. Hepes, DMEM, and lysine-fixable fluorescein dextran at a molecular mass of 70 kDa (D1822) or 2,000 kDa (D7137) were purchased from the Thermo Fisher Scientific Inc. Antibodies included a rat anti–mouse endomucin antibody (14-5858-85; eBioscience), a rabbit anti–mouse UCP1 antibody (10983; Abcam), a rat anti–mouse CD31 antibody (553370; BD Pharmingen), a rat anti–mouse VEGFR1 antibody (MF1; ImClone Systems), and an anti–mouse β-actin antibody (3700S; Cell Signaling Technology).

Cell culture and treatment

3T3F442A preadipocytes were cultured and maintained in DMEM supplemented with 10% FBS, 100 units/ml penicillin, and 100 µg/ml streptomycin. Cell differentiation was induced for 48 h with a DMEM medium containing 850 nM insulin, 0.5 mM IBMX and 0.1 µM DEX, followed by treatment with 850 nM insulin for subsequent 7–10 d. After 10-d induction of differentiation, cells were treated with a rat anti–mouse VEGFR1 (anti-R1) neutralizing antibody or a nonimmune IgG (NIIgG) for 24 and 72 h. UCP1 expression was determined by qPCR.

Pharmacological blocking of VEGFRs

For pharmacological treatment, female, WT C57Bl/6 mice at 7- to 8-wk-old received treatment of a specific anti–mouse VEGFR1 (20 mg/kg, i.p., twice per week, 3–4 times during the entire experiment), an anti-VEGFR2 (20 mg/kg, i.p., twice per week, 3–4 times during the entire experiment), or NIIgG for 10 d (n = 8 mice per group per experiment). These treatment regimens have been known to effectively block their targeted signaling pathways. Treated mice were subjected for metabolic analysis, followed by sacrifice and tissue collection. NIIgG-treated mice using the same regimens served as control groups.

Vascular permeability and perfusion

Vascular perfusion and permeability assays were performed according to our previously published methods (Rouhi et al., 2010; Lim et al., 2012, 2014; Hosaka et al., 2013; Yang et al., 2015, 2016; Seki et al., 2016; Zhang et al., 2016). Briefly, lysine-fixable fluorescein dextrans with molecular masses of 70 kDa or 2,000 kDa were injected into the tail vein of each mouse receiving anti-VEGFR1 or NIIgG treatment as described in the main text. At 5 and 15 min after injections with 2,000 kDa and 70 kDa, respectively, mice were sacrificed, and various adipose depots were immediately fixed with 4% paraformaldehyde overnight for whole-mount staining. The leakage and perfusion were quantified by microscopic-captured images using an Adobe Photoshop CS software program.

Genetic deletion of VEGFR1 in various mouse trains

The global VEGFR1 KO mice were generated by crossing *Flt1*$^{f/f}$ mice with *Rosa26-Cre-ER*^{T2} in a C57Bl/6- and S129-mixture background. Mice were maintained by backcrossing in the C57Bl/6 background (provided by G.-H. Fong, University of Connecticut Health Center, Farmington, CT; Fong et al., 1995). The myeloid cell linage–specific, VEGFR1-deficient mice were generated by crossing the *Flt1*$^{f/f}$ mice with *LysM-Cre* in a C57Bl/6 background (provided by M. Rottenberg, Karolinska Institute, Stockholm, Sweden). The adipocyte-specific, VEGFR1-deficient mice were generated by crossing the *Flt1*$^{f/f}$ mice with *Adipoq-Cre* mice in a C57Bl/6 background (provided by C. Ibanez, Karolinska Institute). The EC-specific, VEGFR1-deficient mice were generated by crossing *Flt1*$^{f/f}$ mice with *Tie2-Cre-ER*^{T2} or *Cdh5-Cre-ER*^{T2} mice in C57Bl/6 backgrounds (generated by A. Bernd and provided by the European Mouse Mutant Archive and R. Adams, Max Planck Institute for Molecular Biomedicine, Muenster, Germany, respectively.). These transgenic strains were identified by genotyping using either ear or tail DNA and a PCR-based method. The specific primer sequences for genotyping are showed in Table S1. The global and EC deletion of the *Vegfr1* gene was achieved by treating mice with tamoxifen.

For generation of the global *Vegfr1* KO strain, the *Flt1*$^{f/f}$*; Rosa26-Cre-ER*^{T2} mice were treated with tamoxifen (2 mg/mouse, i.p., once daily for a consecutive 3 d). Deletion of the

Vegfr1 gene in the *Flt1*$^{f/f}$*;Cdh5-Cre-ER*^{T2} and *Flt1*$^{f/f}$*;Tie2-Cre-ER*^{T2} mice was achieved by tamoxifen induction (2 mg/mouse, i.p., once daily for a consecutive 5 d). About 8–10 d after the last tamoxifen injection, mice were analyzed for metabolism, followed by euthanasia and tissue collection. For the diet-induced obese model, the mice were maintained under standard animal housing conditions and were fed with either standard diet or HFD (D12492; Research Diets Inc.).

Isolation of mature adipocyte fraction (MAF) and stromal vascular fraction (SVF)

The primary MAF and the SVF from subWAT of WT and tamoxifen-treated conditional KO mice were fractioned with a collagenase-digestion–based method (Seki et al., 2016). Tissues were collected, minced, and digested at 37°C for 0.5 h in a collagenase-digestion solution (0.15% collagenase II, 10 mM Hepes, and 5% BSA in DMEM). During digestion, the suspension was triturated with a vortex every 5 min and eventually quenched on ice for 5 min, followed by centrifugation at 300 *g* for 5 min. The floating adipocytes were collected, washed with PBS, and centrifuged at 300 *g* for 10 min. The floating adipocytes were harvested as MAF. The remaining suspension was passed through a 70-μm mesh to remove undigested debris, and effluents were centrifuged at 300 *g* for 10 min. The SVF pellet was washed once with PBS. Cells in SVF were subjected to magnetic-activated cell sorting (MACS) for isolation of either $CD31^+$ or $CD11b^+$ cell populations for assessing KO efficiency. SVF cells were incubated using an anti–mouse CD31 microbeads antibody (130–097-418; Miltenyi Biotec) or a PE-labeled rat anti–mouse CD11b antibody (101208; BioLegend), followed by staining with a magnet-conjugated anti-PE antibody (120-000-294; MACS). Stained cells were separated with MACS columns and an OctoMACS separator (130-042-201 and 130-042-109; MACS) according to the manufacturer's instruction (MACS). Gene expression levels were quantitatively measured by qPCR.

Metabolic measurements

NE-induced thermogenesis and whole-body energy metabolism were quantified by measuring the oxygen consumption of each mouse over defined time points using the Oxymax CLAMS-HC System (Columbus Instruments). The Oxymax machine was kept at 30°C, and the oxygen sensor was heated up for at least 6 h before calibration with the reference gases: 100% nitrogen gas and a mixture of 20.5% O_2 and 0.5% CO_2. For the whole-body energy metabolism, CO_2 and O_2 were measured, and the data were collected every 25 min for each mouse. Metabolic rates were measured as baselines for 24 h before s.c. NE injection (1 mg/kg). The area under the curve (AUC) of the volume of oxygen (VO_2) consumed was calculated for a period of 60 min before NE injection until 160 min after injection. NE-induced thermogenesis for the VEGFRs blockade (Fig. 1 I) was determined by an assessment of oxygen consumption using an open-circuit indirect calorimeter INCA system (Somedic INCA). During the measurement, the mice were anaesthetized, and the basal metabolic rate was measured before NE injection.

Glucose and insulin tolerance tests

Mice were fasted for 6 h during the light phase, with free access to water on the day of the tests. Blood samples collected from the tail vein were used to measure glucose levels with a glucometer (Accu-Chek Aviva; Roche Diagnostics) immediately before and at 15, 30, 60, and 120 min after oral feeding with 1.5 mg glucose and 10 μl/g body weight and i.p. injection of insulin (0.5 U/kg-body weight), respectively.

Blood lipid profiling

FFA, glycerol, cholesterol, and TG were measured with a sensitive assay kit (ab65341, ab65337, ab65359, ab65336; Abcam). Blood insulin was measured with a sensitive ELISA kit according to the manufacturer's instruction (10–1247-01; Mercodia). Blood was collected by cardiac puncture. Mice were fasted for 6 h before sacrifice and blood collection.

Histology and immunohistochemistry

Paraffin-embedded tissue sections in 5-μm thickness were stained with hematoxylin and eosin (H&E) using our standard protocol (Lim et al., 2014; Iwamoto et al., 2015; Seki et al., 2016). For UCP1 and CD31 staining, the paraffin-embedded tissue sections were incubated with a rabbit anti–mouse UCP1 antibody (1:200; Abcam) and a rat anti–mouse CD31 antibody (1:200), followed by staining with a mixture of secondary antibodies comprising an Alexa Fluor 555–labeled goat anti–rat antibody (1:200; Invitrogen) and an Alexa Fluor 649–labeled goat anti–rabbit antibody (1:400; Jackson ImmunoResearch Laboratories Inc.). Positive signals were captured with a fluorescence microscope equipped with a Nikon DS-QilMC camera. A rat anti–mouse VEGFR1 antibody (1:100 dilution in blocking buffer) was used for incubation at 4°C overnight. A secondary goat anti–rat Alexa 555 antibody (A21434; 1:200 dilution; Invitrogen) in blocking buffer was incubated at room temperature for 1 h. For lipid staining, Oil Red O staining was performed according to the BioVision manual. In brief, frozen liver sample was fixed with 4% paraformaldehyde for 30 min, washed with 60% isopropanol, and stained at 37°C with Oil Red O (O1391; Sigma-Aldrich) solution for 15 min. Nuclei were counterstained with hematoxylin for 10 min, mounted with glycerol, and examined under a light microscope.

Whole-mount staining

Whole-mount staining was performed according to our previously published, standard method (Hosaka et al., 2013; Lim et al., 2014; Iwamoto et al., 2015; Seki et al., 2016). Paraformaldehyde-fixed subWAT, visWAT, and interscapular BAT (iBAT) tissue samples were digested with proteinase K (20 μg/ml) for 5 min and blocked with skim milk, followed by staining overnight at 4°C with a rat anti–mouse CD31 antibody (1:200). After rigorous rinsing in PBS, blood vessels were detected with an Alexa Fluor 555–labeled secondary antibody, mounted

in Vectashield mounting medium (Vector Laboratories, Inc.), and stored at −20°C in darkness before examination under a Nikon C1 confocal microscope. Captured images were further analyzed using an Adobe Photoshop CS software program.

RNA isolation, RT-PCR, and qPCR analyses

Total RNA was extracted from cells and tissues using TRIzol (Invitrogen) and GeneJET RNA purification kits according to the manufacturer's instructions. The total RNA was reversely transcribed, and cDNAs were used for PCR and qPCR analyses using the primers listed in Table S1. Samples were stored at −20°C and subjected to qPCR using an ABI Prism 7500 System (Applied Biosystems). Each qPCR sample was performed in triplicate, and the 20-µl reaction contained Fast SYBR Green (4385612; Applied Biosystems), 150 nM forward and reverse primers, and 1 µl cDNA. The qPCR protocol was executed for 40 cycles, and each cycle consisted of denaturation at 95°C for 15 s, annealing at 60°C for 1 min, and extension at 72°C for 1 min.

Western immunoblotting

subWAT tissues were lysed with protein extraction regent (C3228; Sigma-Aldrich) in the presence of a proteinase inhibitor (8340; Sigma-Aldrich) and a phosphatase inhibitor cocktail (5870; Cell Signaling). For VEGFR2 phosphorylation analysis, an equal amount of total protein extract from each tissue lysate was incubated overnight with Protein G-Agarose immunoprecipitation using an anti–phospho-tyrosine antibody (APY03; Cytoskeleton). For CD31 detection, equal amounts of total protein were applied. Tissue samples along with a size marker were loaded on an SDS-PAGE gel (NP0321/NP0323; Life Technologies), followed by transferring onto a nitrocellulose membrane (88018; Thermo Fischer Scientific). After blocking with 3% skim milk, membranes were incubated with a rabbit anti-VEGFR2 (2479; Cell Signaling) antibody, a goat anti-CD31 (AF3628; R&D system) or a mouse anti–β-actin (3700; Cell Signaling) antibody, followed by incubating with an anti–rabbit IRDye-680RD–labeled secondary antibody (926-68073; LI-COR), an anti–goat IRDye 800CW-labeled secondary antibody (926-32214; LI-COR), an anti–mouse IRDye 680RD labeled secondary antibody (926-68072; LI-COR), or an anti–mouse IRDye-800CW–labeled antibody (926-32212; LI-COR). Positive signals were visualized and quantified using Odyssey CLx system (LI-COR).

Statistical analysis

Statistical analysis was performed using the standard Student's *t* test for pair comparisons and ANOVA for multiple factors. Data are presented as means ± SEM of determinants, and values of $P < 0.05$ were deemed statistically significant.

Online supplemental material

Fig. S1 shows that blocking VEGFR1 augments adipose angiogenesis, visWAT browning, and iBAT activation. Fig. S2 shows that genetic elimination of VEGFR1 induces angiogenesis, visWAT browning, and iBAT activation. Fig. S3 shows that endothelial deletion of VEGFR1 augments angiogenesis and visWAT browning in *Flt1$^{f/f}$;Tie2-Cre-ER^{T2}* mice. Fig. S4 shows that deletion of endothelial VEGFR1 in *Flt1$^{f/f}$;Cdh5-Cre-ER^{T2}* mice induces visWAT angiogenesis and browning. Fig. S5 shows that conditional KO of VEGFR1 in ECs of *Flt1$^{f/f}$;Tie2-Cre-ER^{T2}* mice increases antiobesity activity. Table S1 shows the sequences of the primers used in the experiments.

ACKNOWLEDGMENTS

We thank the EC FP7 Capacities Specific Program–funded EMMA service project for providing the *Tie2-Cre-ER^{T2}* mouse line. We thank Dr. Ralf Adams for providing the *Cdh5-Cre-ER^{T2}* mice. We thank Dr. Zhenping Zhu for providing the anti–mouse VEGFR1-neutralizing antibody. We thank Simcere Inc. for providing rabbit anti-VEGF–neutralizing mAb. We thank Dr. Jennifer Honek, Mr. Martin Scherzer, and Mr. Wenyi Zheng at Karolinska Institute for technical assistance and discussions about the project. We thank Dr. Barbara Cannon and Dr. Jan Nedergaard at the Stockholm University, the Arrhenius Laboratories F3, and the Wenner-Grens Institute for assistance with metabolic measurements with an open-circuit indirect calorimeter INCA system.

Y. Cao's laboratory is supported through research grants from the European Research Council advanced grant ANGIOFAT (project 250021), the Swedish Research Council (521-2011-4091), the Swedish Cancer Foundation (11 0564), the Karolinska Institute Foundation, the Karolinska Institute distinguished professor award, the Torsten Soderbergs Foundation (M114/12), the Maud and Birger Gustavsson Foundation, the NOVO Nordisk Foundation (BtN/AIR 4-2432/2014), and the Knut and Alice Wallenberg Foundation. T. Seki was supported by the Scandinavia–Japan Sasakawa Foundation (16-10).

The authors declare no competing financial interests.

Author contributions: Y. Cao generated the initial idea for this study, Y. Cao and T. Seki conceived and designed the experiments and wrote the manuscript. T. Seki, K. Hosaka, C. Fischer, and P. Andersson performed the experiments, analyzed the data, and helped prepare the manuscript. S. Lim, M. Abe, H. Iwamoto, Y. Gao, and X. Wang participated in some of the experimentation and discussed the results. G.-H. Fong provided the *Flt1$^{f/f}$* mice strain.

Submitted: 5 June 2017
Revised: 19 October 2017
Accepted: 5 December 2017

REFERENCES

Asano, A., M. Morimatsu, H. Nikami, T. Yoshida, and M. Saito. 1997. Adrenergic activation of vascular endothelial growth factor mRNA expression in rat brown adipose tissue: implication in cold-induced angiogenesis. *Biochem. J.* 328:179–183. https://doi.org/10.1042/bj3280179

Autiero, M., J. Waltenberger, D. Communi, A. Kranz, L. Moons, D. Lambrechts, J. Kroll, S. Plaisance, M. De Mol, F. Bono, et al. 2003. Role of PlGF in the intra- and intermolecular cross talk between the VEGF receptors Flt1 and Flk1. *Nat. Med.* 9:936–943. https://doi.org/10.1038/nm884

Beck, H., S. Raab, E. Copanaki, M. Heil, A. Scholz, M. Shibuya, T. Deller, M. Machein, and K.H. Plate. 2010. VEGFR-1 signaling regulates the homing of bone marrow-derived cells in a mouse stroke model. *J. Neuropathol. Exp. Neurol.* 69:168–175. https://doi.org/10.1097/NEN.0b013e3181c9c05b

Boulton, M.E., J. Cai, M.B. Grant, and Y. Zhang. 2008. Gamma-secretase regulates VEGFR-1 signalling in vascular endothelium and RPE. *Adv. Exp. Med. Biol.* 613:313–319. https://doi.org/10.1007/978-0-387-74904-4_36

Cao, Y. 2007. Angiogenesis modulates adipogenesis and obesity. *J. Clin. Invest.* 117:2362–2368. https://doi.org/10.1172/JCI32239

Cao, Y. 2009. Positive and negative modulation of angiogenesis by VEGFR1 ligands. *Sci. Signal.* 2:re1. https://doi.org/10.1126/scisignal.259re1

Cao, Y. 2010. Adipose tissue angiogenesis as a therapeutic target for obesity and metabolic diseases. *Nat. Rev. Drug Discov.* 9:107–115. https://doi.org/10.1038/nrd3055

Carmeliet, P., V. Ferreira, G. Breier, S. Pollefeyt, L. Kieckens, M. Gertsenstein, M. Fahrig, A. Vandenhoeck, K. Harpal, C. Eberhardt, et al. 1996. Abnormal blood vessel development and lethality in embryos lacking a single VEGF allele. *Nature.* 380:435–439. https://doi.org/10.1038/380435a0

Després, J.P., and I. Lemieux. 2006. Abdominal obesity and metabolic syndrome. *Nature.* 444:881–887. https://doi.org/10.1038/nature05488

Dong, M., X. Yang, S. Lim, Z. Cao, J. Honek, H. Lu, C. Zhang, T. Seki, K. Hosaka, E. Wahlberg, et al. 2013. Cold exposure promotes atherosclerotic plaque growth and instability via UCP1-dependent lipolysis. *Cell Metab.* 18:118–129. https://doi.org/10.1016/j.cmet.2013.06.003

During, M.J., X. Liu, W. Huang, D. Magee, A. Slater, T. McMurphy, C. Wang, and L. Cao. 2015. Adipose VEGF Links the White-to-Brown Fat Switch With Environmental, Genetic, and Pharmacological Stimuli in Male Mice. *Endocrinology.* 156:2059–2073. https://doi.org/10.1210/en.2014-1905

Ferrara, N., K. Carver-Moore, H. Chen, M. Dowd, L. Lu, K.S. O'Shea, L. Powell-Braxton, K.J. Hillan, and M.W. Moore. 1996. Heterozygous embryonic lethality induced by targeted inactivation of the VEGF gene. *Nature.* 380:439–442. https://doi.org/10.1038/380439a0

Ferrara, N., H.P. Gerber, and J. LeCouter. 2003. The biology of VEGF and its receptors. *Nat. Med.* 9:669–676. https://doi.org/10.1038/nm0603-669

Fong, G.H., J. Rossant, M. Gertsenstein, and M.L. Breitman. 1995. Role of the Flt-1 receptor tyrosine kinase in regulating the assembly of vascular endothelium. *Nature.* 376:66–70. https://doi.org/10.1038/376066a0

Gordts, P.L., E.M. Foley, R. Lawrence, R. Sinha, C. Lameda-Diaz, L. Deng, R. Nock, C.K. Glass, A. Erbilgin, A.J. Lusis, et al. 2014. Reducing macrophage proteoglycan sulfation increases atherosclerosis and obesity through enhanced type I interferon signaling. *Cell Metab.* 20:813–826. https://doi.org/10.1016/j.cmet.2014.09.016

He, J., H. Wang, Y. Liu, W. Li, D. Kim, and H. Huang. 2015. Blockade of vascular endothelial growth factor receptor 1 prevents inflammation and vascular leakage in diabetic retinopathy. *J. Ophthalmol.* 2015:605946. https://doi.org/10.1155/2015/605946

Hiratsuka, S., Y. Maru, A. Okada, M. Seiki, T. Noda, and M. Shibuya. 2001. Involvement of Flt-1 tyrosine kinase (vascular endothelial growth factor receptor-1) in pathological angiogenesis. *Cancer Res.* 61:1207–1213.

Honek, J., T. Seki, H. Iwamoto, C. Fischer, J. Li, S. Lim, N.J. Samani, J. Zang, and Y. Cao. 2014. Modulation of age-related insulin sensitivity by VEGF-dependent vascular plasticity in adipose tissues. *Proc. Natl. Acad. Sci. USA.* 111:14906–14911. https://doi.org/10.1073/pnas.1415825111

Hosaka, K., Y. Yang, T. Seki, M. Nakamura, P. Andersson, P. Rouhi, X. Yang, L. Jensen, S. Lim, N. Feng, et al. 2013. Tumour PDGF-BB expression levels determine dual effects of anti-PDGF drugs on vascular remodelling and metastasis. *Nat. Commun.* 4:2129. https://doi.org/10.1038/ncomms3129

Howangyin, K.Y., I. Zlatanova, C. Pinto, A. Ngkelo, C. Cochain, M. Rouanet, J. Vilar, M. Lemitre, C. Stockmann, B.K. Fleischmann, et al. 2016. Myeloid-Epithelial-Reproductive Receptor Tyrosine Kinase and Milk Fat Globule Epidermal Growth Factor 8 Coordinately Improve Remodeling After Myocardial Infarction via Local Delivery of Vascular Endothelial Growth Factor. *Circulation.* 133:826–839. https://doi.org/10.1161/CIRCULATIONAHA.115.020857

Iwamoto, H., Y. Zhang, T. Seki, Y. Yang, M. Nakamura, J. Wang, X. Yang, T. Torimura, and Y. Cao. 2015. PlGF-induced VEGFR1-dependent vascular remodeling determines opposing antitumor effects and drug resistance to Dll4-Notch inhibitors. *Sci. Adv.* 1:e1400244. https://doi.org/10.1126/sciadv.1400244

Kerber, M., Y. Reiss, A. Wickersheim, M. Jugold, F. Kiessling, M. Heil, V. Tchaikovski, J. Waltenberger, M. Shibuya, K.H. Plate, and M.R. Machein. 2008. Flt-1 signaling in macrophages promotes glioma growth in vivo. *Cancer Res.* 68:7342–7351. https://doi.org/10.1158/0008-5472.CAN-07-6241

Kodack, D.P., E. Chung, H. Yamashita, J. Incio, A.M. Duyverman, Y. Song, C.T. Farrar, Y. Huang, E. Ager, W. Kamoun, et al. 2012. Combined targeting of HER2 and VEGFR2 for effective treatment of HER2-amplified breast cancer brain metastases. *Proc. Natl. Acad. Sci. USA.* 109:E3119–E3127. https://doi.org/10.1073/pnas.1216078109

Li, S., X.L. Zhou, Y.Y. Dang, Y.W. Kwan, S.W. Chan, G.P. Leung, S.M. Lee, and M.P. Hoi. 2015. Basal Flt1 tyrosine kinase activity is a positive regulator of endothelial survival and vascularization during zebrafish embryogenesis. *Biochim. Biophys. Acta.* 1850:373–384. https://doi.org/10.1016/j.bbagen.2014.10.023

Lim, S., J. Honek, Y. Xue, T. Seki, Z. Cao, P. Andersson, X. Yang, K. Hosaka, and Y. Cao. 2012. Cold-induced activation of brown adipose tissue and adipose angiogenesis in mice. *Nat. Protoc.* 7:606–615. https://doi.org/10.1038/nprot.2012.013

Lim, S., Y. Zhang, D. Zhang, F. Chen, K. Hosaka, N. Feng, T. Seki, P. Andersson, J. Li, J. Zang, et al. 2014. VEGFR2-mediated vascular dilation as a mechanism of VEGF-induced anemia and bone marrow cell mobilization. *Cell Reports.* 9:569–580. https://doi.org/10.1016/j.celrep.2014.09.003

Liu, Y., A.D. Berendsen, S. Jia, S. Lotinun, R. Baron, N. Ferrara, and B.R. Olsen. 2012. Intracellular VEGF regulates the balance between osteoblast and adipocyte differentiation. *J. Clin. Invest.* 122:3101–3113. https://doi.org/10.1172/JCI61209

Lyden, D., K. Hattori, S. Dias, C. Costa, P. Blaikie, L. Butros, A. Chadburn, B. Heissig, W. Marks, L. Witte, et al. 2001. Impaired recruitment of bone-marrow-derived endothelial and hematopoietic precursor cells blocks tumor angiogenesis and growth. *Nat. Med.* 7:1194–1201. https://doi.org/10.1038/nm1101-1194

Nguyen, K.D., Y. Qiu, X. Cui, Y.P. Goh, J. Mwangi, T. David, L. Mukundan, F. Brombacher, R.M. Locksley, and A. Chawla. 2011. Alternatively activated macrophages produce catecholamines to sustain adaptive thermogenesis. *Nature.* 480:104–108. https://doi.org/10.1038/nature10653

Otowa, Y., K. Moriwaki, K. Sano, M. Shirakabe, S. Yonemura, M. Shibuya, J. Rossant, T. Suda, Y. Kakeji, and M. Hirashima. 2016. Flt1/VEGFR1 heterozygosity causes transient embryonic edema. *Sci. Rep.* 6:27186. https://doi.org/10.1038/srep27186

Robciuc, M.R., R. Kivelä, I.M. Williams, J.F. de Boer, T.H. van Dijk, H. Elamaa, F. Tigistu-Sahle, D. Molotkov, V.M. Leppänen, R. Käkelä, et al. 2016. VEGFB/VEGFR1-Induced Expansion of Adipose Vasculature Counteracts Obesity and Related Metabolic Complications. *Cell Metab.* 23:712–724. https://doi.org/10.1016/j.cmet.2016.03.004

Rouhi, P., L.D. Jensen, Z. Cao, K. Hosaka, T. Länne, E. Wahlberg, J.F. Steffensen, and Y. Cao. 2010. Hypoxia-induced metastasis model in embryonic zebrafish. *Nat. Protoc.* 5:1911–1918. https://doi.org/10.1038/nprot.2010.150

Sander, L.E., F. Obermeier, U. Dierssen, D.C. Kroy, A.K. Singh, U. Seidler, K.L. Streetz, H.H. Lutz, W. Müller, F. Tacke, and C. Trautwein. 2008. Gp130 signaling promotes development of acute experimental colitis by facilitating early neutrophil/macrophage recruitment and activation. *J. Immunol.* 181:3586–3594. https://doi.org/10.4049/jimmunol.181.5.3586

Seki, T., K. Hosaka, S. Lim, C. Fischer, J. Honek, Y. Yang, P. Andersson, M. Nakamura, E. Näslund, S. Ylä-Herttuala, et al. 2016. Endothelial PDGF-CC regulates angiogenesis-dependent thermogenesis in beige fat. *Nat. Commun.* 7:12152. https://doi.org/10.1038/ncomms12152

Shaked, Y., E. Henke, J.M. Roodhart, P. Mancuso, M.H. Langenberg, M. Colleoni, L.G. Daenen, S. Man, P. Xu, U. Emmenegger, et al. 2008. Rapid chemotherapy-induced acute endothelial progenitor cell mobilization: implications for antiangiogenic drugs as chemosensitizing agents. *Cancer Cell*. 14:263–273. https://doi.org/10.1016/j.ccr.2008.08.001

Shan, B., X. Wang, Y. Wu, C. Xu, Z. Xia, J. Dai, M. Shao, F. Zhao, S. He, L. Yang, et al. 2017. The metabolic ER stress sensor IRE1α suppresses alternative activation of macrophages and impairs energy expenditure in obesity. *Nat. Immunol.* 18:519–529. https://doi.org/10.1038/ni.3709

Shibuya, M. 2006. Vascular endothelial growth factor receptor-1 (VEGFR-1/Flt-1): a dual regulator for angiogenesis. *Angiogenesis.* 9:225–230, discussion :231. https://doi.org/10.1007/s10456-006-9055-8

Shibuya, M. 2014. VEGF-VEGFR Signals in Health and Disease. *Biomol. Ther. (Seoul)*. 22:1–9. https://doi.org/10.4062/biomolther.2013.113

Spiegelman, B.M., and J.S. Flier. 2001. Obesity and the regulation of energy balance. *Cell*. 104:531–543. https://doi.org/10.1016/S0092-8674(01)00240-9

Sun, K., I. Wernstedt Asterholm, C.M. Kusminski, A.C. Bueno, Z.V. Wang, J.W. Pollard, R.A. Brekken, and P.E. Scherer. 2012. Dichotomous effects of VEGF-A on adipose tissue dysfunction. *Proc. Natl. Acad. Sci. USA*. 109:5874–5879. https://doi.org/10.1073/pnas.1200447109

Sung, H.K., K.O. Doh, J.E. Son, J.G. Park, Y. Bae, S. Choi, S.M. Nelson, R. Cowling, K. Nagy, I.P. Michael, et al. 2013. Adipose vascular endothelial growth factor regulates metabolic homeostasis through angiogenesis. *Cell Metab.* 17:61–72. https://doi.org/10.1016/j.cmet.2012.12.010

Tang, W., D. Zeve, J.M. Suh, D. Bosnakovski, M. Kyba, R.E. Hammer, M.D. Tallquist, and J.M. Graff. 2008. White fat progenitor cells reside in the adipose vasculature. *Science.* 322:583–586. https://doi.org/10.1126/science.1156232

Tonello, C., A. Giordano, V. Cozzi, S. Cinti, M.J. Stock, M.O. Carruba, and E. Nisoli. 1999. Role of sympathetic activity in controlling the expression of vascular endothelial growth factor in brown fat cells of lean and genetically obese rats. *FEBS Lett*. 442:167–172. https://doi.org/10.1016/S0014-5793(98)01627-5

Tran, K.V., O. Gealekman, A. Frontini, M.C. Zingaretti, M. Morroni, A. Giordano, A. Smorlesi, J. Perugini, R. De Matteis, A. Sbarbati, et al. 2012. The vascular endothelium of the adipose tissue gives rise to both white and brown fat cells. *Cell Metab.* 15:222–229. https://doi.org/10.1016/j.cmet.2012.01.008

Welford, A.F., D. Biziato, S.B. Coffelt, S. Nucera, M. Fisher, F. Pucci, C. Di Serio, L. Naldini, M. De Palma, G.M. Tozer, and C.E. Lewis. 2011. TIE2-expressing macrophages limit the therapeutic efficacy of the vascular-disrupting agent combretastatin A4 phosphate in mice. *J. Clin. Invest.* 121:1969–1973. https://doi.org/10.1172/JCI44562

Witte, L., D.J. Hicklin, Z. Zhu, B. Pytowski, H. Kotanides, P. Rockwell, and P. Böhlen. 1998. Monoclonal antibodies targeting the VEGF receptor-2 (Flk1/KDR) as an anti-angiogenic therapeutic strategy. *Cancer Metastasis Rev.* 17:155–161. https://doi.org/10.1023/A:1006094117427

Xue, Y., N. Petrovic, R. Cao, O. Larsson, S. Lim, S. Chen, H.M. Feldmann, Z. Liang, Z. Zhu, J. Nedergaard, et al. 2009. Hypoxia-independent angiogenesis in adipose tissues during cold acclimation. *Cell Metab.* 9:99–109. https://doi.org/10.1016/j.cmet.2008.11.009

Yang, X., Y. Zhang, K. Hosaka, P. Andersson, J. Wang, F. Tholander, Z. Cao, H. Morikawa, J. Tegnér, Y. Yang, et al. 2015. VEGF-B promotes cancer metastasis through a VEGF-A-independent mechanism and serves as a marker of poor prognosis for cancer patients. *Proc. Natl. Acad. Sci. USA*. 112:E2900–E2909. https://doi.org/10.1073/pnas.1503500112

Yang, Y., Y. Zhang, Z. Cao, H. Ji, X. Yang, H. Iwamoto, E. Wahlberg, T. Länne, B. Sun, and Y. Cao. 2013. Anti-VEGF- and anti-VEGF receptor-induced vascular alteration in mouse healthy tissues. *Proc. Natl. Acad. Sci. USA*. 110:12018–12023. https://doi.org/10.1073/pnas.1301331110

Yang, Y., Y. Zhang, H. Iwamoto, K. Hosaka, T. Seki, P. Andersson, S. Lim, C. Fischer, M. Nakamura, M. Abe, et al. 2016. Discontinuation of anti-VEGF cancer therapy promotes metastasis through a liver revascularization mechanism. *Nat. Commun.* 7:12680. https://doi.org/10.1038/ncomms12680

Zhang, Y., Y. Yang, K. Hosaka, G. Huang, J. Zang, F. Chen, Y. Zhang, N.J. Samani, and Y. Cao. 2016. Endocrine vasculatures are preferable targets of an antitumor ineffective low dose of anti-VEGF therapy. *Proc. Natl. Acad. Sci. USA*. 113:4158–4163. https://doi.org/10.1073/pnas.1601649113

Zimmet, P., K.G. Alberti, and J. Shaw. 2001. Global and societal implications of the diabetes epidemic. *Nature.* 414:782–787. https://doi.org/10.1038/414782a